Geophysical Research Letters

RESEARCH LETTER
10.1029/2023GL107757

Repeated and Long-Lasting Fault Activation on Amazonian Mars as Demonstrated by Tectonically Induced Landslides

S. Z. Woodley[1], P. Fawdon[1], M. R. Balme[1], and D. A. Rothery[1]

[1]School of Physical Sciences, The Open University, Milton Keynes, UK

Key Points:

- A large shortening structure in western Arabia Terra is associated with four landslides of various degradation states inside a single crater
- We propose that the landslides were tectonically-triggered and formed at different times during the Middle to Late Amazonian epoch
- The shortening structure shows evidence of repeated, long-lasting, and recent compressional tectonic activity in western Arabia Terra

Supporting Information:

Supporting Information may be found in the online version of this article.

Correspondence to:

S. Z. Woodley,
savana.woodley@open.ac.uk

Citation:

Woodley, S. Z., Fawdon, P., Balme, M. R., & Rothery, D. A. (2024). Repeated and long-lasting fault activation on Amazonian Mars as demonstrated by tectonically induced landslides. *Geophysical Research Letters*, *51*, e2023GL107757. https://doi.org/10.1029/2023GL107757

Received 8 DEC 2023
Accepted 13 APR 2024

Abstract We identify and analyze a large shortening structure (surface expression of a thrust fault) in western Arabia Terra, Mars, exhibiting recent, repeated, and long-lasting tectonic activity. Where the fault system deforms Marsabit crater rim, four landslides with differing degradation states extend onto the crater floor. We propose these were triggered by episodic re-activation of the thrust system. Using a morphological map and crater size frequency statistics we show that the fault system experienced at least four landslide-inducing events during the Middle to Late Amazonian. We note that 1.4 km total displacement on the fault plane must have required many events to accumulate if motion was by brittle failure rather than continuous creep. The current understanding of tectonic activity and stress-sources since 3.6 Ga, cannot account for these repeated and large Amazonian marsquakes—suggesting revaluation of sources of stress to account for a more active and complex Amazonian tectonic history.

Plain Language Summary We identify a large fault system, called a shortening structure, that has been repeatedly active during the last 2 billion years. This is suggested by a series of landslides with a variety of degradation states. These originate from where a large-scale shortening structure deforms the wall of Marsabit crater. We propose these were triggered by at least four large tectonic events. The shortening structure has a scarp face height of about 700 m, implying that about 1.4 km of movement has occurred along the fault; requiring tens to thousands of marsquakes to accumulate. Our evidence that multiple marsquakes occurred "recently" (in the last 2 billion years) is important because Mars is thought to have been barely tectonically active during this time. This raises questions about the regional/global processes responsible for recent tectonic activity of this magnitude which would have likely re-activated other local tectonic structures. Our study shows that repeated and long-lasting tectonic activity occurred in the last 2 billion years, and finding more young tectonic structures would help to better understand the spatial and temporal extent of Mars' recent tectonic history.

1. Introduction

The surface record of tectonic deformation on Mars represents crustal stress, which reflects the planet's geodynamic evolution. Shortening structures are the surface expression of thrust-faults with various degrees of folding (morphologically described as wrinkle ridges and lobate scarps; Klimczak et al., 2019). Martian compressional tectonic activity is hypothesized to have peaked during the late Noachian and early Hesperian (3.8–3.6 Ga; Hartmann & Neukum, 2001; Michael, 2013), based on observed shortening structure abundance found in units of this age (e.g., Tanaka et al., 1991; Watters, 1993). Thermal evolution models suggest that, following an early period of rapid cooling of Mars' interior (e.g., Schubert et al., 1992), secular cooling and resulting global contraction occurred from the early Noachian through to the present day (Andrews-Hanna et al., 2008; Hauck & Phillips, 2002; Schubert & Spohn, 1990). Although Mars is still tectonically active in the present day (e.g., Banerdt et al., 2020), evidence of middle-late Amazonian (<1.2 Ga; Michael, 2013) shortening structures is sparse. Proposed Amazonian (<3.4 Ga; Michael, 2013) shortening structures are limited to volcanic regions such as Alba Patera (R. C. Anderson et al., 2001; Bouley et al., 2018) and Tyrrhena Patera (Goudy et al., 2005), or associated with large basins such as Utopia and Isidis Planitiae (Tanaka et al., 2003; Tanaka, Robbins, et al., 2014).

Ages of shortening structures have previously been inferred using two methods. First, ages of individual structures are assigned based on their cross-cutting relationships with surface units (R. C. Anderson et al., 2001, 2008; Bouley et al., 2018; Knapmeyer et al., 2006; Watters, 1993). The unit age represents a maximum formation age, because a structure can be any age younger than the surface it deforms. Second, buffered crater counting (BCC;

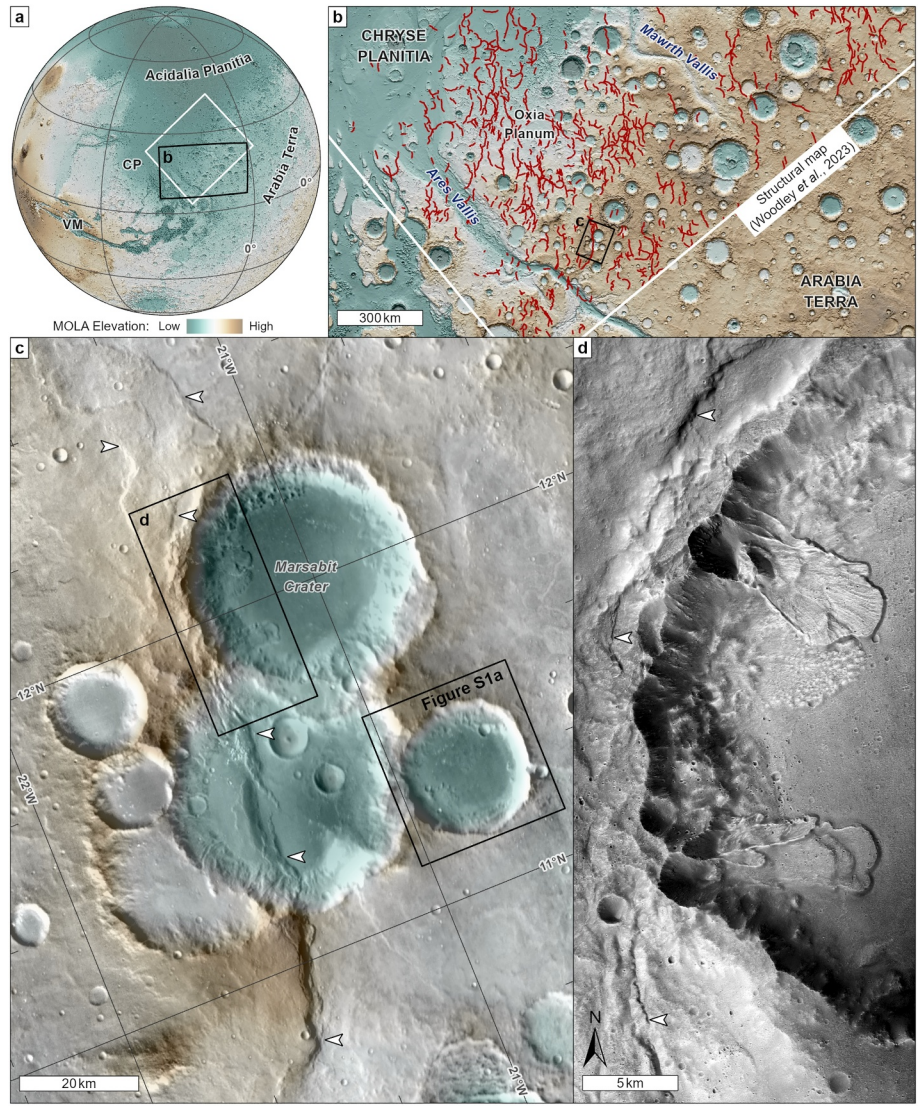

Figure 1. The location of the study area in western Arabia Terra, Mars, and the series of landslides. (a) Global setting. "CP" is Chryse Planitia and "VM" is Valles Marineris. (b) Regional setting, with red lines showing shortening structures (Woodley et al., 2023). (c) Study area in western Arabia Terra. Arrows mark a large shortening structure. THEMIS Day IR. (d) The western rim of Marsabit, with four landslides. Arrows show the shortening structure deforming the crater wall. CTX global mosaic (Dickson et al., 2023).

Kneissl et al., 2015) can be used to assign ages of structure populations (Ruj et al., 2019; Ruj & Kawai, 2021). However, this method is limited by the number of intersecting impact craters and the assumption that all structures within the population have the same age. Furthermore, by assigning a single formation age, neither method captures a comprehensive formation history of shortening structures which could be reactivated multiple times, as on Earth, with displacement accumulating over millions to billions of years.

We identify a large shortening structure in western Arabia Terra (Figure 1) that shows evidence of repeated, long-lasting, and "recent" tectonic activity. The shortening structure has a height of ~700 m and deforms two large impact craters, including the wall of Marsabit crater where a series of four landslides originate from alcoves at the displaced crater wall and extend onto the crater floor. Contrasting amounts of degradation of each landslide indicate that they formed at different times; we suggest that these landslides were triggered by tectonic activity. The shortening structure was re-activated in at least four landslide-inducing tectonic events but probably resulted also from a great many smaller marsquakes (as required for the ~1.4 km displacement of the fault system) that did not trigger landslides. We present a morphological map of the tectonically-deformed crater system and constrain

the timing of tectonic events using crater size-frequency distributions (CSFD) of the four landslides and the crater floor of Marsabit, and BCC of the shortening structure. Our study provides context for the tectonic history of western Arabia Terra and, more generally, insight into Amazonian tectonic activity on Mars.

2. Study Area

Western Arabia Terra lies close to Mars' highland-lowland transitional boundary, east of Chryse and Acidalia Planitia (Figure 1). The region comprises predominantly heavily cratered Noachian and Hesperian terrain (Tanaka, Skinner, et al., 2014), with a complex geological history and stratigraphy that includes the deposits of extensive river systems (Davis et al., 2016, 2023; Fawdon et al., 2022). Tectonic deformation has occurred throughout the region, as evidenced by widespread shortening structures (formation ages unknown; Woodley et al., 2023). The study area (10–13°N and 20–23°W; Figure 1c) lies between Ares and Mawrth Valles, and about ~400 km southeast of Oxia Planum, the landing site of the ExoMars rover (Quantin-Nataf et al., 2021; Vago et al., 2017). The study area comprises a cluster of six 15–40 km diameter impact craters, including ~40 km diameter Marsabit. Marsabit and a similar sized adjacent (unnamed) crater to its SSW are tectonically deformed by a large shortening structure system.

3. Data and Methods

To produce a geomorphological map of the study area, we used the ~6 m/pixel Context Camera (CTX; Malin et al., 2007) global mosaic (Dickson et al., 2023) and individual CTX images. We used a stereographic projection centered on the study area (11.8°N, 21.2°W) to minimize cartographic distortion. Geomorphological units and linear features were digitized in *ArcGIS Pro 3.1.0*, at 1:50,000 scale with 100 m vertex spacing.

We determined the CSFDs of the four landslides in Marsabit, the Marsabit crater floor, and the southern section of the shortening structure. Two additional landslides in the ~20 km diameter crater southeast of Marsabit are not analyzed, as they are too degraded and affected by secondary cratering (Figure S1 in Supporting Information S1). Using the *CraterTools* add-in (Kneissl et al., 2011, 2015) in *ArcGIS 10.5.0* and individual CTX images, we digitized the count areas at 1:20,000 scale and superposing impact craters at 1:5,000 scale. For the BCC of the shortening structure (Kneissl et al., 2015), the steep scarp face forms the count area. Where the scarp face is shadowed, the image exposure was increased to improve visibility—although some shadow zones remained. We used a simple buffer approach (buffer width = one crater radius, 1R), meaning that only superimposed craters were digitized (Kneissl et al., 2015), as using the 2R or 3R approach introduces more uncertainty due to the difficulty of determining relative ages of ejecta blankets.

We analyzed the CSFDs and the BCC with *Craterstats 2.0* (Michael & Neukum, 2010) to derive model ages. The resulting model ages are best-fit estimates, but have significant uncertainties, due to small count areas (<1,000 km^2), sample size, and crater diameters (Hartmann, 2005; Warner et al., 2015). The model ages of the landslides represent the timing of tectonic events on the shortening structure if they were tectonically triggered. The model age of the Marsabit floor reflects its most recent resurfacing (not the age of the impact) and constrains the maximum formation age of the landslides that overlie it. The model age of the shortening structure represents the cessation of the most recent detectable activity associated with that structure.

4. Observations and Results

4.1. Morphological Map

We identified six morphological units (surrounding plains excluded) associated with the series of six impact craters in the study area (Figure 2). For each crater, the *Crater Wall unit* (*Cw*; Figure 2f), the *Crater Floor unit* (*Cf*; Figure 2g), and the *Ejecta unit* (*Ej*; Figure 2d) would have formed simultaneously during impact. Relative crater formation ages of C1 (oldest crater) to C6 (youngest crater), with Marsabit being C3, is based on superposition (e.g., C2 superposes C1 so must postdate it) and degradation state (e.g., C5 has preserved *Ej*, C4 does not so probably predates it). The *Crater wall slump unit* (*Cs*; Figure 2e) lies at the bottom of the crater wall and has a shallower slope (~20° instead of ~30° slope angle) and a more bumpy/uneven surface than *Cw*. It occurs in Marsabit and C4, like the *Landslide unit* (*Ld*; Figure 2c). *Ld* comprises six deposits, four in Marsabit and two in C4. We refer to the northernmost landslide in Marsabit as L1, counting down to the southernmost landslide which we refer to as L4 (Figures 3b and 3c). The most degraded deposits (L2 in Marsabit and the two in C4) have

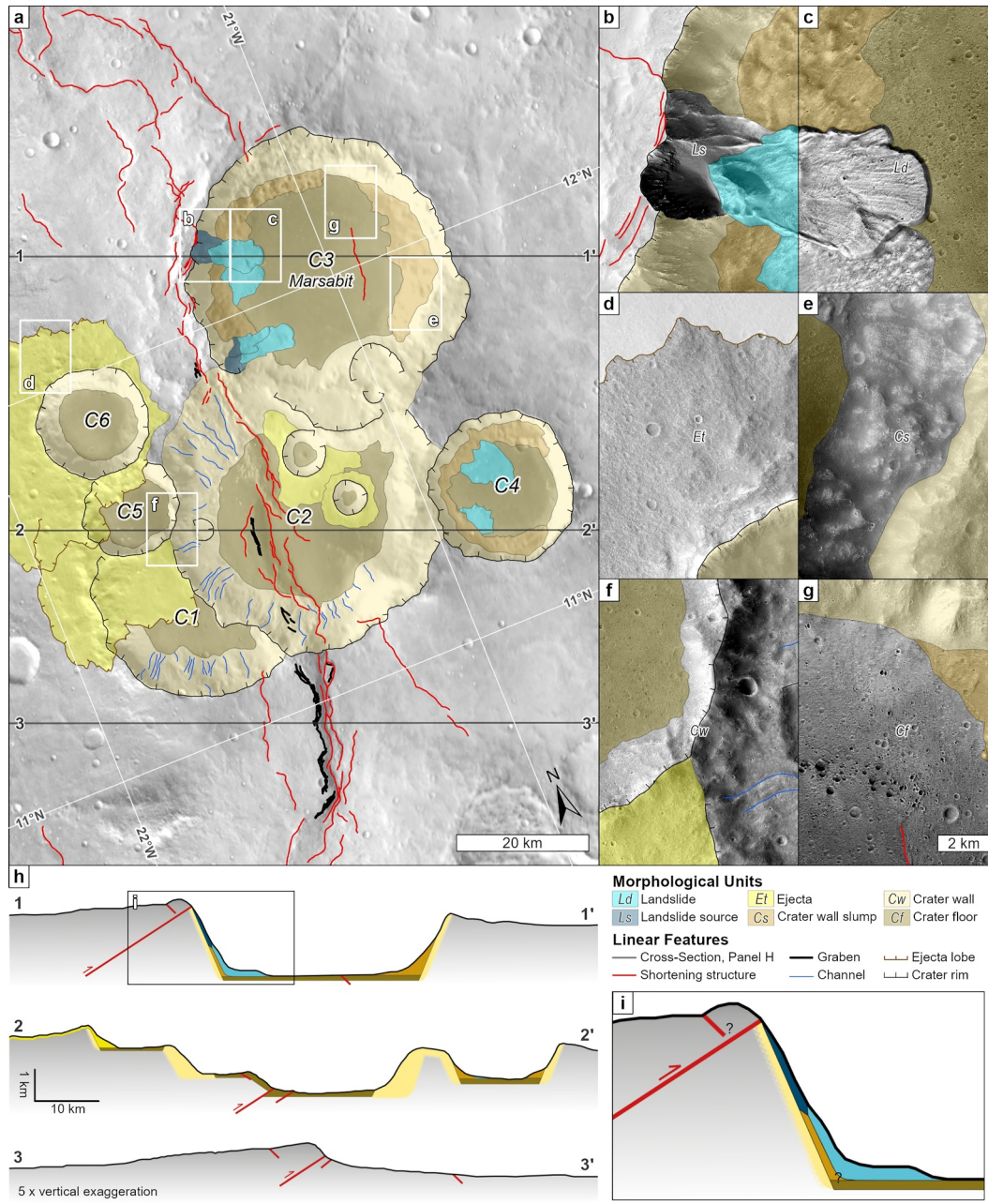

Figure 2. Map and cross-sections of the study area. (a) Morphological map showing impact and landslide units (subjacent plains are not mapped). THEMIS Day IR basemap. (b)–(g) Type locations of the morphological map units. The scale is the same in all panels (scale bar in panel g). CTX mosaic (Dickson et al., 2023), with the subject unit left uncolored and surrounding units colored. (h)–(i) Cross-sections 1–1', 2–2', and 3–3', with MOLA surface topography. Subsurface contacts and unit thickness are inferred from the topography and observed stratigraphic relationships. Fault dip angles and sub-surface structure are inferred and simplified.

inferred and very eroded contacts with *Cs*. However, L1, L3, and L4 originate from the *Landslide source unit* (*Ls*; Figure 2b), from alcoves in the steep western wall of Marsabit where a shortening structure deforms the crater wall.

A large shortening structure system deforms the study area, trending generally SSW with an assumed WNW fault plane dip (Figure 2). The shortening structure has a measured vertical displacement of ~700 m in the plains south of C2, ~500 m where it deforms the C2 floor, and the western rim of Marsabit is ~400 m higher than its eastern

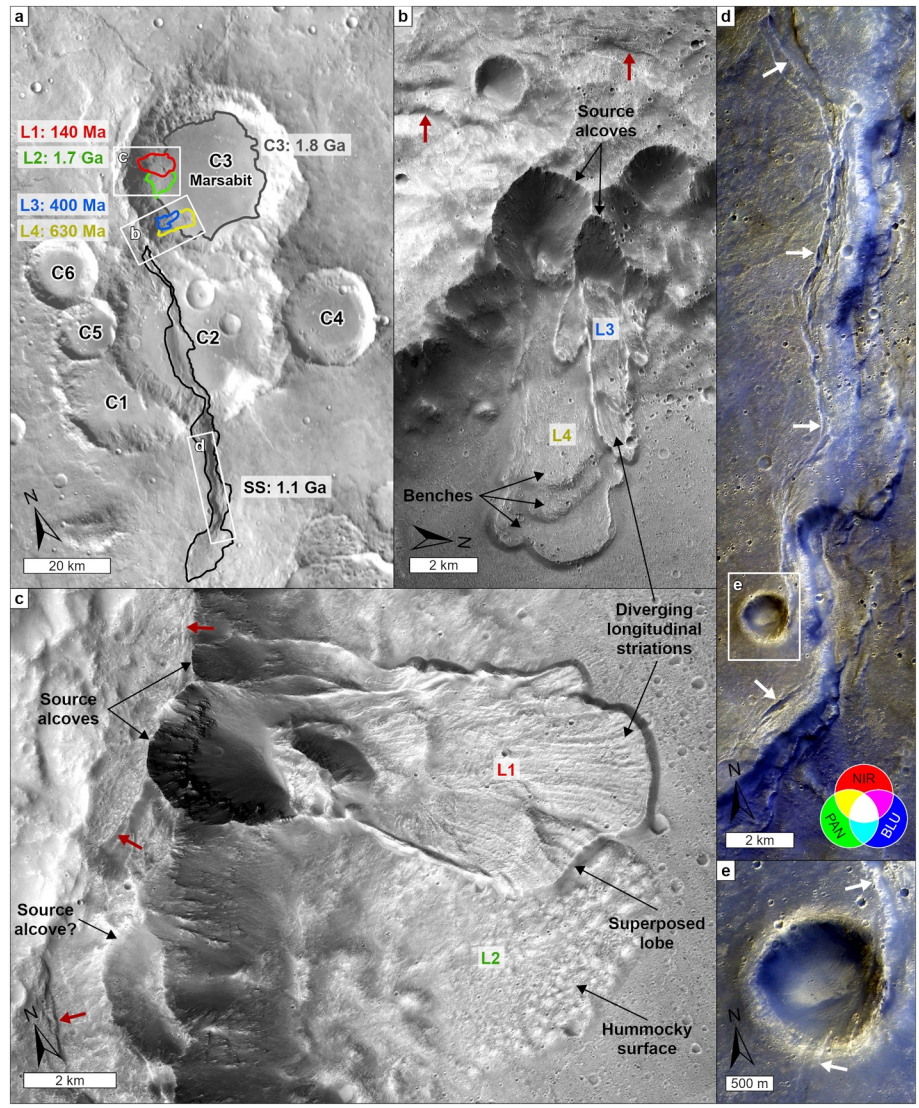

Figure 3. Features in the study area. (a) C1–C6 show the formation sequence of impact craters. Polygons show the extent of the count area for CSFD analysis. THEMIS Day IR basemap. (b)–(c) The four Marsabit landslides. Red arrows indicate linear features interpreted as faults, small grabens, and/or tension cracks. CTX mosaic (Dickson et al., 2023). (d) Scarp face of the shortening structure exposing light toned deposits in CaSSIS Near IR (NIR, ~850 nm), Pancromatic (PAN, ~676.5 nm) and Blue (BLU, ~480.5 nm) image MY37_022982_012_0 (Thomas et al., 2017; Tornabene et al., 2017). Parallel to the main structure, are crenulations at the scarp base and grabens at the scarp crest including deformation of (e) a ~1.5 km diameter crater.

rim. The shortening structure's leading edge has a scalloped and crenulated appearance. There are small grabens oriented parallel to the main structure's crest (Figure 3d); they have a minimally degraded appearance, and a series of grabens can be seen deforming a ~1.5 km impact crater (Figure 3e). The shortening structure deforms the western rim of Marsabit, appearing to have directly deformed the original rim section that now forms the L1 alcove, and lies within 2 km of the source alcoves of L3 and L4.

The four landslides (L1–L4) in Marsabit each have different morphologies (Figures 3b and 3c). L1 comprises a main elongated lobe-shaped deposit and an adjacent narrow deposit to its northeast (Figure 3c). The narrow deposit has well-defined lateral levées; it originates from a separate alcove northeast of the main alcove, before merging downslope with the main deposit. The main deposit originates from a well-defined alcove, with possible tension cracks or faults along it. The scar is only partially emptied, as material remains on the steep crater wall

(Figures 2i and 3c). The surface of the deposit is characterized by diverging longitudinal striations and lateral levées. The southwest section of the deposit superposes L2 (Figure 3c).

L2 is a lobe-shaped deposit with a hummocky surface appearance (Figure 3c). Its source alcove is not clearly identifiable and L2 is too degraded to have visible levées leading to its alcove, however there is a possible source alcove on the crater wall above the deposit (Figure 3c).

L3 comprises an elongated narrow deposit overlying a smaller deposit on either side, with all three evidently sourced from the same alcove and therefore likely resulting from a single event (Figure 3b). The deposits have lateral levées and the larger deposit has longitudinal striations on its surface. The three lobes originate in an alcove that cross-cuts the source alcove of L4, and the southern section of the deposit superposes L4 (Figure 3b).

L4 is comprised of an elongated lobe-shaped deposit with three benches, the most distal extending to the terminus (Figure 3b). The surface has longitudinal striations, although they are not as well defined as those of L1 and L3. The deposit originates in an alcove, with linear structures that look like scarps with grabens to the southwest (Figures 1d and 3b).

There are two further landslides (L5 and L6) that occur along the NW rim of C4 (Figure 2a and Figure S1 in Supporting Information S1). The western rim of C4 is located 20–30 km from the main shortening structure and ∼16 km from a smaller shortening structure to the southwest. The northernmost landslide in C4, L5, is the largest (38.5 km^2) and most degraded landslide. There is no obvious source alcove along the C4 rim and the contact with *Cs* is gradational and obscured by secondary craters. The southernmost landslide, L6, has a fan-shaped appearance and is also heavily degraded with merely the margins of the terminal lobes preserved.

The relative ages of the landslides are reflected by superposition relationships, demonstrating L1 on top of L2, and L3 on top of L4. This sequence is consistent with their morphology, on the basis that this reflects the degree of degradation and thus landslide age. L1 and its source alcove have the freshest appearance and so L1 is youngest, followed by L3, L4, L2, L6, and lastly L5 which is the most degraded and oldest.

4.2. Landslide and Shortening Structure Ages

We determined the CSFD of the four Marsabit landslides and the floor of Marsabit, count areas are shown in Figure 3 and the associated craters and CSFD plots are supplied in Figures S2 and S3 in Supporting Information S1. L1 has a ∼30.6 km^2 count area and we digitize 276 impact craters. We found a best-fit isochron of 140 ± 10 Ma for 175 craters with diameters between 30 and 170 m. L2 has a ∼21.5 km^2 count area and we digitize 446 impact craters. We found a best-fit isochron of 1.7 ± 1 Ga for 2 craters with diameters between 250 and 400 m and 300 ± 20 Ma for 301 craters with diameters between 30 and 80 m. L3 has a ∼10.3 km^2 count area and we digitize 218 impact craters (25 secondary craters excluded). We found a best-fit isochron of 400 ± 40 Ma for 112 craters with diameters between 35 and 70 m. L4 has a ∼20.8 km^2 count area and we digitize 366 impact craters. We found a best-fit isochron of 630 ± 80 Ma for 63 craters with diameters between 60 and 150 m. The crater floor of Marsabit has a ∼493.1 km^2 count area and we digitize 460 impact craters. We found a best-fit isochron of 1.8 ± 0.2 Ga for 115 craters with diameters between 200 and 900 m. The CSFD ages indicate that the Marsabit floor is the oldest, followed by L2, L4, L3, and L1 is the youngest. This matches the age relationships seen in superposition observations and degradational morphology.

Lastly, we determined the CSFD of the shortening structure using BCC. The structure's scarp face forms a ∼272.3 km^2 count area, comprising intercrater plains and C2 crater floor. We found a best-fit isochron of 1.1 ± 0.3 Ga for 17 craters with diameters between 250 and 700 m.

5. Interpretation and Discussion

5.1. Landslide Trigger Mechanism

Numerous processes have been proposed to trigger landslides on Mars including impact events, high relief and slope instability, groundwater and cryosphere processes, and tectonic activity (e.g., Crosta et al., 2018; Guimpier et al., 2021; Kumar et al., 2019; Roback & Ehlmann, 2021). The four landslides in Marsabit were previously recorded as rock avalanches in the martian landslide inventory (Crosta et al., 2018), but neither trigger mechanisms nor ages were discussed. Impact cratering can trigger landslides in multiple ways. High-energy impacts cause ground-shaking which can trigger landslides; for example, a 1–2 km diameter impact crater causes a

marsquake with a moment magnitude of 5.0–5.5 (Teanby, 2015; Teanby & Wookey, 2011). Additionally, impacts located close to steep slopes (e.g., valley walls or crater rims) can destabilize the slopes, directly triggering landslides (Crosta et al., 2018). In fact, pre-disposing factors such as high-relief topography and impact gardening are significant controlling factors (Crosta et al., 2014), with relief being the primary control on global landslide distribution (Roback & Ehlmann, 2021). Surface or sub-surface ice/water may also play a role in the formation of landslides (De Blasio, 2011; Watkins et al., 2020), as their presence can decrease slope stability and trigger landslides (Crosta et al., 2018). Lastly, landslides can be triggered by tectonic activity, either by ground shaking as a result of seismic waves or by direct ground deformation causing slope failure (e.g., Keefer, 1984). Large tectonically-triggered landslides have been identified in Valles Marineris (Kumar et al., 2019) and smaller ones in circum-Chryse outflow channels (Guimpier et al., 2021). Kumar et al. (2019) propose that landslides can be seismically triggered by tectonically-induced marsquakes if $M_W \geq 5$ (focal depth ≤2 km); this is consistent with magnitudes of terrestrial tectonically-triggered landslides (Keefer, 1984).

We suggest that the four landslides in Marsabit formed as the tectonic shortening structure deformed the crater rim, causing rim slope failure (direct) and/or seismic ground shaking (indirect) that triggered the landslides. Although it is conceivable that some of them have different trigger mechanisms, their apparent morphological, stratigraphic, and contextual similarities make this improbable. There is a clear spatial association between the four landslides and the shortening structure; the L1 alcove directly deforms the leading edge of the shortening structure and L3 and L4 lie within ∼2 km of the structure. Therefore, we suggest that the four landslides in Marsabit formed as the shortening structure deformed the crater rim, causing rim slope failure (direct) and/or seismic ground shaking (indirect) that triggered the landslides. Although it is conceivable that some of the landslides were triggered by impact-induced ground shaking, the absence of nearby craters displaying minimally degraded ejecta blankets (as would be expected due to low Amazonian erosion rates; Golombek et al., 2006) suggest that this is unlikely. Liquid water/ice related activity as a trigger mechanism is also improbable, as the landslides formed during the Middle-Late Amazonian epoch, long after aqueous processes were active at scale (e.g., Carr & Head, 2010). The two landslides in C4 do not share the same close spatial association with the shortening structure as L1–L4. Although this rules-out a direct tectonic trigger by slope failure, tectonic activity could have indirectly triggered them by seismic ground shaking. The C4 rim where L5 and L6 originate, lies ∼16 km from a small shortening structure and 20–30 km from the main shortening structure (Figure 2). On Earth, large earthquakes (M_W 8–9) can trigger landslides >200 km from the epicenter, and for smaller earthquakes (M_W 6–8) 50–100 km from the epicenter (Keefer, 1984).

The shortening structure in the study area is the largest regional structure (Woodley et al., 2023) with a maximum scarp height of ∼700 m. Assuming a planar fault geometry with a 30° dip angle (e.g., E. M. Anderson, 1905) and pure dip-slip, the "true" displacement of this shortening structure is 1.4 km. A lower dip angle would result in a larger displacement (e.g., 2.0 km for a 20° dip) and if displacement is horizontally accommodated by folding then this would also result in a larger displacement than calculated. The calculated displacement is far too large to result from a single event. The largest tectonic marsquake detected by InSight is M_W 4.7 (S1222a; Fernando et al., 2023), assuming a displacement equivalent to the 2007 M_W 4.7 Katanning earthquake (∼42 cm; Dawson et al., 2008), a 1.4 km displacement would require about 3300 M_W 4.7 marsquakes. Even if (unrealistically) large marsquakes formed the shortening structure, it would still require 58 marsquakes—each equivalent to the 2011 M_W 9.0 Tohoku-Oki earthquake (∼24 m maximum slip; Sato et al., 2011). The total 1.4 km displacement probably results from a great many smaller marsquakes that did not trigger landslides in addition to the larger ones that did.

5.2. The Timing of the Landslides and Tectonic Activity

If the landslides were tectonically-triggered and formed co-seismically, as common on Earth (Keefer, 1984), then these landslides are indicators of palaeo-marsquakes. The landslide ages of 140 Ma, 400 Ma, 630 Ma, and 1.7 Ga (L1, L3, L4, and L2 respectively) therefore reflect the occurrence of fault re-activation along the associated shortening structure system and that episodic tectonic activity occurred in western Arabia Terra during the middle-late Amazonian. Landslides previously reported from the middle-late Amazonian triggered by seismic shaking (e.g., Kumar et al., 2019; Quantin et al., 2004), are found in younger terrain such as steep-sided valleys in Valles Marineris or outflow channels associated with extensional high-angle faults. The shortening structure has a BCC model age of 1.1 ± 0.3 Ga for the southern scarp area (Figure 3a). As a record of the cessation of the most recent tectonic activity associated with the shortening structure (e.g., Ruj & Kawai, 2021), this reflects only

cessation of activity capable of "resetting" the crater count by erasing all impact craters on the scarp face. More recent tectonic activity of the scarp is supported by the presence of small grabens that occur parasitically on the large shortening structure, resembling equivalent examples that indicate recent tectonism on Mercury (Man et al., 2023).

5.3. Implications for Tectonic Activity

We identify seismically induced landslides in Noachian highland terrain, with tectonic activity associated with a shortening structure as the trigger mechanism. This recent and substantial tectonic activity in an unexpected location (i.e., not associated with a volcanic center) means we must revaluate hypotheses about sources and accumulation of stress in the martian crust. Compressional martian tectonic activity is caused by global contraction, Tharsis-related-stress, dichotomy-related stress, or regional/local stresses (e.g., Watters, 1993).

The north-south orientation of the shortening structure and others in western Arabia Terra (Woodley et al., 2023) coincide with orientations of late Noachian and early Hesperian Tharsis-circumferential structures (Watters, 1993). However, Amazonian Tharsis-related shortening structures appear largely limited to Alba Patera (Bouley et al., 2018), so Tharsis-related re-activation of the shortening structure in the study area is unlikely. Stresses related to the dichotomy boundary and the isostatic adjustment of the highlands and lowlands were proposed by Ruj and Kawai (2021) for the formation of Amazonian wrinkle ridges in Amenthes Planum, and Watters (1993) proposed that dichotomy-related stresses produced dichotomy parallel shortening structures. Widespread exhumation of Noachian terrain has occurred across the dichotomy in western Arabia Terra (McNeil et al., 2022; Quantin-Nataf et al., 2021), which may have contributed to Hesperian dichotomy-related stresses. Although, the shortening structure in the study area is oriented oblique to the dichotomy boundary (NE-SW, Figure 1), it could have been re-activated by dichotomy-related stresses.

Secular cooling of Mars' interior causing global contraction is hypothesized to have began in the early Noachian and continued through to the present day, based on thermal evolution models (Andrews-Hanna et al., 2008; Schubert et al., 1992; Schubert & Spohn, 1990). Global contraction estimates from globally mapped fault populations are several times smaller than predicted by thermal evolution models and find that of Mars' total contractional strain, a late Noachian and Early Hesperian pulse makes up ~59% (Knapmeyer et al., 2008; Nahm & Schultz, 2011). Steady cooling and contraction in the Amazonian is supported by thermal evolution models (e.g., Hauck & Phillips, 2002; Plesa et al., 2015), although recent work based on accumulated fault density and cumulative strain contradicts steady state models of thermal evolution and suggests episodic mantle evolution, with negligible contractional strain from the late Hesperian onwards (Andrews-Hanna & Broquet, 2023). Under this scenario, the re-activation of the shortening structure in the study area throughout the Amazonian epoch could not be attributed to global contraction.

Based on the large size of the shortening structure and the number of events required to form it, it seems likely that the fault system formed over a long period; originally forming during the Noachian (it deforms *eNh*; Tanaka, Skinner, et al., 2014) and re-activating continuously until at least the Late Amazonian. No singular stress source is thought to have been active over this entire time span, suggesting that multiple stress sources would have contributed to reactivating the shortening structure over time. The stress-sources that are responsible for the formation of this shortening structure and its continual re-activation during the Amazonian would have been regionally active; thus there should be more evidence of Amazonian compressional tectonic activity.

6. Conclusions

We identify a large shortening structure in western Arabia Terra, Mars, that shows evidence of recent, repeated, and long-lasting tectonic activity. The shortening structure deforms the western rim of Marsabit crater, where four landslides originate from alcoves and extend onto the crater floor. We produce a geomorphological map of the study area and conduct crater size-frequency distribution analyses on the four landslides and buffered crater counts of the shortening structure.

We propose that the landslides are tectonically-induced; forming co-tectonically during re-activation of the shortening structure thrust fault. The landslides have model ages of 140 ± 10 Ma, 400 ± 40 Ma, 630 ± 80 Ma, and 1.7 ± 1 Ga. This suggests that the shortening structure was tectonically-active multiple times (at least 4) during the Middle to Late Amazonian epoch.

To account for the large displacement of the shortening structure, it would have had to be active episodically over a long period of time; we suggest that it formed during the Noachian circumferentially to Tharsis, and since then has been continuously reactivated thanks to multiple stress sources, including global contraction and dichotomy-related stresses. Our study represents the first direct evidence of Amazonian compressional tectonic activity in western Arabia Terra and suggests that our current insight into Mars' tectonic history and thermal heating models do not adequately account for the observed high level of Amazonian tectonic activity in the ancient highlands.

Data Availability Statement

For CSFD analysis, we used Craterstats 2.0 software (https://www.geo.fu-berlin.de/en/geol/fachrichtungen/planet/software/_content/software/craterstats.html) and the CraterTools add-in (https://www.geo.fu-berlin.de/en/geol/fachrichtungen/planet/software/_content/software/cratertools.html), both available from the Freie Universität Berlin. All the data used is freely available. CTX data is available from the Murray Lab (https://murray-lab.caltech.edu/CTX/) or Mars Image Explorer (https://viewer.mars.asu.edu/viewer/ctx#T = 0). HRSC data can be downloaded from the Freie Universitat Berlin (https://maps.planet.fu-berlin.de/#map = 3/2074498.35/0). CaSSIS data is available from the Physics Institute University of Bern (https://observations.cassis.unibe.ch/). Data is available from the PDS Annex or USGS Astrogeology Science Center for THEMIS (https://pds-imaging.jpl.nasa.gov/volumes/ody.html or https://astrogeology.usgs.gov/search/map/Mars/Odyssey/THEMIS-IR-Mosaic-ASU/Mars_MO_THEMIS-IR-Day_mosaic_global_100m_v12) and MOLA gridded data (https://pds-geosciences.wustl.edu/missions/mgs/mola.html or https://astrogeology.usgs.gov/search/map/Mars/Global-Surveyor/MOLA/Mars_MGS_MOLA_ClrShade_merge_global_463m).

Acknowledgments

We gratefully acknowledge funding from STFC grant ST/V50693X/1 and The Open University STEM Faculty (SZW), UK Space Agency ST/W002736/1 (PF), and ST/R001413/1 (MRB). We thank all the scientists and engineers who built CTX and have operated it for over a decade at Malin Space Science Systems and the Jet Propulsion Laboratory, and the Murray Lab for compiling the CTX mosaic data set. The authors wish to thank the CaSSIS spacecraft and instrument engineering teams. CaSSIS is a project of the University of Bern and funded through the Swiss Space Office via ESA's PRODEX programme. The instrument hardware development was also supported by the Italian Space Agency (ASI) (ASI-INAF agreement no. I/2020-17-HH.0), INAF/Astronomical Observatory of Padova, and the Space Research Center (CBK) in Warsaw. Support from SGF (Budapest), the University of Arizona (Lunar and Planetary Lab.) and NASA are also gratefully acknowledged. Operations support from the UK Space Agency under grant ST/R003025/1 is also acknowledged. This research has made use of the USGS Integrated Software for Imagers and Spectrometers (ISIS).

References

Anderson, E. M. (1905). The dynamics of faulting. In *Geological Survey*. Oliver & Boyd.

Anderson, R. C., Dohm, J. M., Golombek, M. P., Haldemann, A. F. C., Franklin, B. J., Tanaka, K. L., et al. (2001). Primary centers and secondary concentrations of tectonic activity through time in the western hemisphere of Mars. *Journal of Geophysical Research*, *106*(E9), 20563–20585. https://doi.org/10.1029/2000JE001278

Anderson, R. C., Dohm, J. M., Haldemann, A. F. C., Pounders, E., Golombek, M. P., & Castano, A. (2008). Centers of tectonic activity in the eastern hemisphere of Mars. *Icarus*, *195*(2), 537–546. https://doi.org/10.1016/j.icarus.2007.12.027

Andrews-Hanna, J. C., & Broquet, A. (2023). The history of global strain and geodynamics on Mars. *Icarus*, *395*(115476), 115476. https://doi.org/10.1016/j.icarus.2023.115476

Andrews-Hanna, J. C., Zuber, M. T., & Hauck, S. A. (2008). Strike-slip faults on Mars: Observations and implications for global tectonics and geodynamics. *Journal of Geophysical Research*, *113*(E8), 8002. https://doi.org/10.1029/2007JE002980

Banerdt, W. B., Smrekar, S. E., Banfield, D., Giardini, D., Golombek, M., Johnson, C. L., et al. (2020). Initial results from the InSight mission on Mars. *Nature Geoscience*, *13*(3), 183–189. https://doi.org/10.1038/s41561-020-0544-y

Bouley, S., Baratoux, D., Paulien, N., Missenard, Y., & Saint-Bézar, B. (2018). The revised tectonic history of Tharsis. *Earth and Planetary Science Letters*, *488*, 126–133. https://doi.org/10.1016/J.EPSL.2018.02.019

Carr, M. H., & Head, J. W. (2010). Geologic history of Mars. *Earth and Planetary Science Letters*, *294*(3–4), 185–203. https://doi.org/10.1016/j.epsl.2009.06.042

Crosta, G. B., Frattini, P., Valbuzzi, E., & De Blasio, F. V. (2018). Introducing a new inventory of large martian landslides. *Earth and Space Science*, *5*(4), 89–119. https://doi.org/10.1002/2017EA000324

Crosta, G. B., Utili, S., De Blasio, F. V., & Castellanza, R. (2014). Reassessing rock mass properties and slope instability triggering conditions in Valles Marineris, Mars. *Earth and Planetary Science Letters*, *388*, 329–342. https://doi.org/10.1016/J.EPSL.2013.11.053

Davis, J. M., Balme, M., Grindrod, P. M., Williams, R. M. E., & Gupta, S. (2016). Extensive Noachian fluvial systems in Arabia Terra: Implications for early Martian climate. *Geology*, *44*(10), 847–850. https://doi.org/10.1130/G38247.1

Davis, J. M., Balme, M. R., Fawdon, P., Grindrod, P. M., Favaro, E. A., Banham, S. G., & Thomas, N. (2023). Ancient alluvial plains at Oxia Planum, Mars. *Earth and Planetary Science Letters*, *601*, 117904. https://doi.org/10.1016/J.EPSL.2022.117904

Dawson, J., Cummins, P., Tregoning, P., & Leonard, M. (2008). Shallow intraplate earthquakes in Western Australia observed by Interferometric Synthetic Aperture Radar. *Journal of Geophysical Research*, *113*(B11). https://doi.org/10.1029/2008JB005807

De Blasio, F. V. (2011). Landslides in Valles Marineris (Mars): A possible role of basal lubrication by sub-surface ice. *Planetary and Space Science*, *59*(13), 1384–1392. https://doi.org/10.1016/J.PSS.2011.04.015

Dickson, J. L., Ehlmann, B. L., Kerber, L. H., & Fassett, C. I. (2023). Release of the global CTX Mosaic of Mars: An experiment in information-preserving image data processing. In *54th Lunar and planetary science conference* (p. 2353). https://doi.org/10.1029/2006JE002808

Fawdon, P., Balme, M., Davis, J., Bridges, J., Gupta, S., & Quantin-Nataf, C. (2022). Rivers and lakes in Western Arabia Terra: The fluvial catchment of the ExoMars 2022 Rover landing site. *Journal of Geophysical Research: Planets*, *127*(2), e2021JE007045. https://doi.org/10.1029/2021JE007045

Fernando, B., Daubar, I. J., Charalambous, C., Grindrod, P. M., Stott, A., Al Ateqi, A., et al. (2023). A Tectonic origin for the largest marsquake observed by InSight. *Geophysical Research Letters*, *50*(20), e2023GL103619. https://doi.org/10.1029/2023GL103619

Golombek, M. P., Grant, J. A., Crumpler, L. S., Greeley, R., Arvidson, R. E., Bell, J. F., et al. (2006). Erosion rates at the Mars Exploration Rover landing sites and long-term climate change on Mars. *Journal of Geophysical Research*, *111*(E12), 12–22. https://doi.org/10.1029/2006JE002754

Goudy, C. L., Schultz, R. A., & Gregg, T. K. P. (2005). Coulomb stress changes in Hesperia Planum, Mars, reveal regional thrust fault reactivation. *Journal of Geophysical Research*, *110*(E10), 1–12. https://doi.org/10.1029/2004JE002293

Guimpier, A., Conway, S. J., Mangeney, A., Lucas, A., Mangold, N., Peruzzetto, M., et al. (2021). Dynamics of recent landslides (<20 My) on Mars: Insights from high-resolution topography on Earth and Mars and numerical modelling. *Planetary and Space Science*, *206*, 105303. https://doi.org/10.1016/J.PSS.2021.105303

Hartmann, W. K. (2005). Martian cratering 8: Isochron refinement and the chronology of Mars. *Icarus*, *174*(2), 294–320. https://doi.org/10.1016/J.ICARUS.2004.11.023

Hartmann, W. K., & Neukum, G. (2001). Cratering chronology and the evolution of Mars. *Space Science Reviews*, *96*(1/4), 165–194. https://doi.org/10.1023/A:1011945222010

Hauck, S. A., & Phillips, R. J. (2002). Thermal and crustal evolution of Mars. *Journal of Geophysical Research*, *107*(E7), 6-1–6-19. https://doi.org/10.1029/2001JE001801

Keefer, D. K. (1984). Landslides caused by earthquakes. *GSA Bulletin*, *95*(4), 406–421. https://doi.org/10.1130/0016-7606(1984)95<406:lcbe>2.0.co;2

Klimczak, C., Byrne, P. K., Sengör, C. A. M., & Solomon, S. C. (2019). Principles of structural geology on rocky planets. *Canadian Journal of Earth Sciences*, *56*(12), 1437–1457. https://doi.org/10.1139/cjes-2019-0065

Knapmeyer, M., Oberst, J., Hauber, E., Wählisch, M., Deuchler, C., & Wagner, R. (2006). Working models for spatial distribution and level of Mars' seismicity. *Journal of Geophysical Research*, *111*(E11006). https://doi.org/10.1029/2006JE002708

Knapmeyer, M., Schneider, S., Misun, M., Wählisch, M., & Hauber, E. (2008). An extended global inventory of Mars surface faults. *Geophysical Research Abstracts*, *10*, 11006. https://doi.org/10.1029/2006JE002708

Kneissl, T., Michael, G. G., Platz, T., & Walter, S. H. G. (2015). Age determination of linear surface features using the Buffered Crater Counting approach – Case studies of the Sirenum and Fortuna Fossae graben systems on Mars. *Icarus*, *250*, 384–394. https://doi.org/10.1016/J.ICARUS.2014.12.008

Kneissl, T., Van Gasselt, S., & Neukum, G. (2011). Map-projection-independent crater size-frequency determination in GIS environments—New software tool for ArcGIS. *Planetary and Space Science*, *59*(11–12), 1243–1254. https://doi.org/10.1016/J.PSS.2010.03.015

Kumar, P. S., Krishna, N., Prasanna Lakshmi, K. J., Raghukanth, S. T. G., Dhabu, A., & Platz, T. (2019). Recent seismicity in Valles Marineris, Mars: Insights from young faults, landslides, boulder falls and possible mud volcanoes. *Earth and Planetary Science Letters*, *505*, 51–64. https://doi.org/10.1016/J.EPSL.2018.10.008

Malin, M. C., Bell, J. F., Cantor, B. A., Caplinger, M. A., Calvin, W. M., Clancy, R. T., et al. (2007). Context Camera investigation on board the Mars reconnaissance orbiter. *Journal of Geophysical Research*, *112*(5), 5–9. https://doi.org/10.1029/2006JE002808

Man, B., Rothery, D. A., Balme, M. R., Conway, S. J., & Wright, J. (2023). Widespread small grabens consistent with recent tectonism on Mercury. *Nature Geoscience*, *16*(10), 856–862. https://doi.org/10.1038/s41561-023-01281-5

McNeil, J. D., Fawdon, P., Balme, M. R., Coe, A. L., & Thomas, N. (2022). Mounds in Oxia Planum: The burial and exhumation of the ExoMars Rover landing site. *Journal of Geophysical Research: Planets*, *127*(11), e2022JE007246. https://doi.org/10.1029/2022JE007246

Michael, G. G. (2013). Planetary surface dating from crater size–frequency distribution measurements: Multiple resurfacing episodes and differential isochron fitting. *Icarus*, *226*(1), 885–890. https://doi.org/10.1016/J.ICARUS.2013.07.004

Michael, G. G., & Neukum, G. (2010). Planetary surface dating from crater size–frequency distribution measurements: Partial resurfacing events and statistical age uncertainty. *Earth and Planetary Science Letters*, *294*(3–4), 223–229. https://doi.org/10.1016/J.EPSL.2009.12.041

Nahm, A. L., & Schultz, R. A. (2011). Magnitude of global contraction on Mars from analysis of surface faults: Implications for martian thermal history. *Icarus*, *211*(1), 389–400. https://doi.org/10.1016/j.icarus.2010.11.003

Plesa, A. C., Tosi, N., Grott, M., & Breuer, D. (2015). Thermal evolution and Urey ratio of Mars. *Journal of Geophysical Research: Planets*, *120*(5), 995–1010. https://doi.org/10.1002/2014JE004748

Quantin, C., Allemand, P., Mangold, N., & Delacourt, C. (2004). Ages of Valles Marineris (Mars) landslides and implications for canyon history. *Icarus*, *172*(2), 555–572. https://doi.org/10.1016/J.ICARUS.2004.06.013

Quantin-Nataf, C., Carter, J., Mandon, L., Thollot, P., Balme, M., Volat, M., et al. (2021). Oxia Planum: The landing site for the ExoMars "rosalind Franklin" Rover mission: Geological context and Prelanding Interpretation. *Astrobiology*, *21*(3), 345–366. https://doi.org/10.1089/ast.2019.2191

Roback, K. P., & Ehlmann, B. L. (2021). Controls on the global distribution of martian landslides. *Journal of Geophysical Research: Planets*, *126*(5), e2020JE006675. https://doi.org/10.1029/2020JE006675

Ruj, T., & Kawai, K. (2021). A global investigation of wrinkle ridge formation events; Implications towards the thermal evolution of Mars. *Icarus*, *369*, 114625. https://doi.org/10.1016/J.ICARUS.2021.114625

Ruj, T., Komatsu, G., Pasckert, J. H., & Dohm, J. M. (2019). Timings of early crustal activity in southern highlands of Mars: Periods of crustal stretching and shortening. *Geoscience Frontiers*, *10*(3), 1029–1037. https://doi.org/10.1016/J.GSF.2018.05.016

Sato, M., Ishikawa, T., Ujihara, N., Yoshida, S., Fujita, M., Mochizuki, M., & Asada, A. (2011). Displacement above the hypocenter of the 2011 Tohoku-Oki earthquake. *Science*, *332*(6036), 1395. https://doi.org/10.1126/SCIENCE.1207401/SUPPL_FILE/SATO.SOM.PDF

Schubert, G., Soloman, S. C., Turcotte, D. L., Drake, M. J., & Sleep, N. H. (1992). Origin and thermal evolution of Mars. In H. H. Kieffer, B. M. Jakosky, C. W. Snyder, & M. S. Matthews (Eds.), *Mars* (pp. 147–183). University of Arizona Press.

Schubert, G., & Spohn, T. (1990). Thermal history of Mars and the sulfur content of its core. *Journal of Geophysical Research*, *95*(B9), 95–109. https://doi.org/10.1029/JB095iB09p14095

Tanaka, K. L., Golombek, M. P., & Banerdt, W. B. (1991). Reconciliation of stress and structural histories of the Tharsis region of Mars. *Journal of Geophysical Research*, *96*(E1), 15617–15633. https://doi.org/10.1029/91JE01194

Tanaka, K. L., Robbins, S. J., Fortezzo, C. M., Skinner, J. A., & Hare, T. M. (2014). The digital global geologic map of Mars: Chronostratigraphic ages, topographic and crater morphologic characteristics, and updated resurfacing history. *Planetary and Space Science*, *95*, 11–24. https://doi.org/10.1016/J.PSS.2013.03.006

Tanaka, K. L., Skinner, J. A., Dohm, J. M., Irwin, R. P., Kolb, E. J., Fortezzo, C. M., et al. (2014). *Geologic map of Mars*. USGS Scientific Investigations Map 3292.

Tanaka, K. L., Skinner, J. A., Hare, T. M., Joyal, T., & Wenker, A. (2003). Resurfacing history of the northern plains of Mars based on geologic mapping of Mars Global Surveyor data. *Journal of Geophysical Research*, *108*(E4), 1–32. https://doi.org/10.1029/2002JE001908

Teanby, N. A. (2015). Predicted detection rates of regional-scale meteorite impacts on Mars with the InSight short-period seismometer. *Icarus*, *256*, 49–62. https://doi.org/10.1016/J.ICARUS.2015.04.012

Teanby, N. A., & Wookey, J. (2011). Seismic detection of meteorite impacts on Mars. *Physics of the Earth and Planetary Interiors*, *186*(1–2), 70–80. https://doi.org/10.1016/J.PEPI.2011.03.004

Thomas, N., Cremonese, G., Ziethe, R., Gerber, M., Brändli, M., Bruno, G., et al. (2017). The colour and Stereo surface imaging system (CaSSIS) for the ExoMars Trace Gas orbiter. *Space Science Reviews*, *212*(3–4), 1897–1944. https://doi.org/10.1007/S11214-017-0421-1/FIGURES/24

Tornabene, L. L., Seelos, F. P., Pommerol, A., Thomas, N., Caudill, C. M., Becerra, P., et al. (2017). Image simulation and assessment of the colour and spatial capabilities of the colour and stereo surface imaging system (CaSSIS) on the ExoMars Trace Gas Orbiter. *Space Science Reviews*, *214*(1), 1–61. https://doi.org/10.1007/S11214-017-0436-7

Vago, J. L., Westall, F., Coates, A. J., Jaumann, R., Korablev, O., Ciarletti, V., et al. (2017). Habitability on early Mars and the search for biosignatures with the ExoMars Rover. *Astrobiology*, *17*(6–7), 471–510. https://doi.org/10.1089/ast.2016.1533

Warner, N. H., Gupta, S., Calef, F., Grindrod, P., Boll, N., & Goddard, K. (2015). Minimum effective area for high resolution crater counting of martian terrains. *Icarus*, *245*, 198–240. https://doi.org/10.1016/J.ICARUS.2014.09.024

Watkins, J. A., Ehlmann, B. L., & Yin, A. (2020). Spatiotemporal evolution, mineralogical composition, and transport mechanisms of long-runout landslides in Valles Marineris, Mars. *Icarus*, *350*, 113836. https://doi.org/10.1016/J.ICARUS.2020.113836

Watters, T. R. (1993). Compressional tectonism on Mars. *Journal of Geophysical Research*, *98*(E9), 17049–17060. https://doi.org/10.1029/93je01138

Woodley, S. Z., Fawdon, P., Balme, M. R., & Rothery, D. A. (2023). Map of tectonic shortening structures in Chryse Planitia and Arabia Terra, Mars. *Journal of Maps*, *19*(1). https://doi.org/10.1080/17445647.2023.2251514